

Preliminary performance results of the Weighted Fourier Phase Slope centroiding method for Shack-Hartmann wavefront sensors obtained with the OOMAO simulator

Chulani, H. M.^{*a}, Rodríguez-Ramos, J. M.^b

^aInstituto de Astrofísica de Canarias, Cl. Vía Láctea, s/n, La Laguna, Canary Islands, 38205 Spain

^bFaculty of Physics, University of La Laguna, Avda. Astrofísico Fco. Sánchez, s/n, Canary Islands, 38206 Spain

ABSTRACT

"Weighted Fourier Phase Slope" is a centroiding method that operates in the Fourier domain. It directly computes the Fourier phase slope at discrete spatial frequencies without the intermediate step of working out the phase, and then applies a weight to the slope at each frequency which is application's geometry dependent. The number of spatial frequencies involved is a few, and the computational requirement is significantly lesser than for the Cross-Correlation centroiding method. The algorithm has been introduced in the OOMAO (Object Oriented Matlab for Adaptive Optics) simulator's Shack-Hartmann wavefront sensor object, and its performance compared with Thresholded Centre of Gravity and Cross-Correlation centroiding methods, for natural guide star open loop compensated adaptive optics systems. These preliminary results show a sensitiveness and sky coverage performance similar to Cross-Correlation's, with an improvement over the Thresholded Centre of Gravity of 0.6 to 0.7 in the limiting star magnitude.

Keywords: adaptive optics, simulation, Shack-Hartmann wavefront sensor, centroiding method, Fourier domain

1. INTRODUCTION

Shack-Hartmann wavefront sensors (SHWFS) continue to be the most widely employed and to have the most matured technology amongst wavefront sensors to be found in astronomy applications. With the advent of Multi Object Adaptive Optics (MOAO) systems, which operate in an open loop correction configuration, wavefront sensors are posed with the requirement of maintaining their sensitiveness in low light level conditions while sensing a larger Field of View (FoV) than in traditional closed loop systems, in order to cope with the uncorrected atmospheric turbulence dynamic range. For SHWFS's, this requirement directly falls over the centroiding method employed to estimate the tilt at the subpupil level from the spot's position at the focal plane image, and therefore justifies the revision of traditional centroiding methods and the proposal of new ones.

Hardware speed and processing capabilities are in continuous growth. Hundreds and even thousands of GFlops of processing power of modern GPU's (Graphical Processing Units), for example, invite us to move from the simple Centre of Gravity (CoG) based traditional centroiding methods, which work in the subpupil image domain, towards more robust methods that work in transformed domains where denoising filters are more easily applied.

In this paper we present some preliminary results of the performance of a centroiding method formulated as an optimized Bayesian estimator in the Fourier domain, for Shack-Hartmann wavefront sensors. Results are obtained by simulation of an open loop configured Adaptive Optics (AO) system in which a Natural Guide Star (NGS) is the sensing light source. Its performance is compared with the Thresholded Centre of Gravity (TCoG) and Cross-Correlation (CC) centroiding methods. We have called it the *Weighted Fourier Phase Slope* (WFPS) algorithm.

2. DESCRIPTION OF THE WEIGHTED FOURIER PHASE SLOPE ALGORITHM

The formulation of the WFPS has already been presented and validated as a tilt estimation method at the subpupil level of SHWFS's¹. Basically, the algorithm first calculates the slopes, or derivatives with respect to both spatial frequency axes,

* Hareh.Chulani@iac.es; Phone: (+34) 922 605200 #5476

of the image's Fourier phase, and then averages these slopes with optimized weights in order to obtain the centroid's horizontal and vertical coordinates in the image domain.

It can be shown that, for a subpupil image I_{xy} , the following expressions hold for its Fourier phase slopes^{2, 3}:

$$\begin{aligned} \frac{\partial}{\partial \omega_x} \left(\arg \left(\mathcal{F}\{I_{xy}\} \Big|_{\omega_x, \omega_y} \right) \right) &= -\operatorname{Re} \left\{ \frac{\mathcal{F}\{xI_{xy}\} \Big|_{\omega_x, \omega_y}}{\mathcal{F}\{I_{xy}\} \Big|_{\omega_x, \omega_y}} \right\} \\ \frac{\partial}{\partial \omega_y} \left(\arg \left(\mathcal{F}\{I_{xy}\} \Big|_{\omega_x, \omega_y} \right) \right) &= -\operatorname{Re} \left\{ \frac{\mathcal{F}\{yI_{xy}\} \Big|_{\omega_x, \omega_y}}{\mathcal{F}\{I_{xy}\} \Big|_{\omega_x, \omega_y}} \right\} \end{aligned} \quad (1)$$

with x and y being the horizontal and vertical coordinates in the image domain, $\mathcal{F}\{\cdot\}$ being the Fourier transform, $\omega_x = 2\pi f_x$, $\omega_y = 2\pi f_y$, f_x and f_y being the spatial frequencies in the horizontal and vertical axes, respectively, $\operatorname{Re}\{\cdot\}$ being the operation of taking the real part and $\arg(\cdot)$ being the "unwrapped" phase, such that the result is a continuous function of the spatial frequencies. Note that expression (1) allows us to compute the Fourier phase slope of image I_{xy} , as a negated real part of a quotient of Fourier transforms, without the need of explicitly computing the phase and unwrapping it. Taking into account that negative slopes imply positive image displacements, and that the discretized versions of the Fourier transforms are in practice employed, expression (1) gives place to:

$$\begin{aligned} C_{k,l}^x &= \operatorname{Re} \left\{ \frac{2D_FFT\{xI_{xy}\} \Big|_{k,l}}{2D_FFT\{I_{xy}\} \Big|_{k,l}} \right\} \\ C_{k,l}^y &= \operatorname{Re} \left\{ \frac{2D_FFT\{yI_{xy}\} \Big|_{k,l}}{2D_FFT\{I_{xy}\} \Big|_{k,l}} \right\} \end{aligned} \quad (2)$$

with $2D_FFT\{\cdot\}$ being the bi-dimensional Fast Fourier Transform, and $C_{k,l}^x$ and $C_{k,l}^y$ being the horizontal and vertical image displacements evaluated at the discretized spatial frequencies determined by the integer k and l indexes.

For a perfectly symmetric and well sampled spot in a noiseless image and with infinite field of view, the corresponding phase in the Fourier domain would be planar, and so, any two entries, one from each of the pair of image displacement matrices in expression (2), would define a perfect estimator of the phase tilt in the subpupil. However, for a real non-symmetric pixelized spot in a noisy image with limited FoV, the same pair of entries would be a noisy estimator of the phase tilt, and so the following expression holds:

$$\begin{aligned} C_v^x &= H \times C^x + E^x \\ C_v^y &= H \times C^y + E^y \end{aligned} \quad (3)$$

where C_v^x and C_v^y are rearrangements of $C_{k,l}^x$ and $C_{k,l}^y$ in column vector format, respectively; C^x and C^y are the spot's displacement in pixels related to the true* horizontal and vertical phase tilts at the subpupil, respectively; H is an observation vector with the same size as C_v^x or C_v^y with unity entries; and, finally, E^x and E^y are error vectors. The size of these vectors correspond to the number of selected spatial frequencies, N_f . Assuming Gaussian probability distributions for displacements and errors, and disregarding the knowledge of the *a priori* means of displacements C^x and C^y , the proposed WFPS algorithm is a Bayesian MAP (Maximum a Posteriori) estimator of C^x and C^y given by:

$$\begin{aligned} \hat{C}_{WFPS}^x &= (H^T V_{E^x}^{-1} H)^{-1} (H^T V_{E^x}^{-1} C_v^x) \\ \hat{C}_{WFPS}^y &= (H^T V_{E^y}^{-1} H)^{-1} (H^T V_{E^y}^{-1} C_v^y) \end{aligned} \quad (4)$$

* "True" tilt at the subpupil is the tilt we are interested in estimating, such as Z-Tilt (Zernike tilt) or G-Tilt (mean of the phase gradient).

V_{E^x} and V_{E^y} are the covariance matrices of errors E^x and E^y . Their role is to give more weight to the cleanest or less noisy displacement measurements in C_v^x and C_v^y . Moreover, they take advantage of the strong correlation of the errors at neighbour spatial frequencies to cancel out noise in an optimized manner. Expression (4) can finally be rearranged as weighted combinations of the displacements $C_{k,l}^x$ and $C_{k,l}^y$, calculated at the different spatial frequencies in the Fourier domain as phase slopes:

$$\begin{aligned}\hat{C}_{WFPS}^x &= \sum_{\substack{k,l \\ N_f}}^{N_f} W_{k,l}^x \times C_{k,l}^x \\ \hat{C}_{WFPS}^y &= \sum_{k,l} W_{k,l}^y \times C_{k,l}^y\end{aligned}\tag{5}$$

with multiplication in (5) being element-wise. Weight matrices $W_{k,l}^x$ and $W_{k,l}^y$ are rearrangements into matrix format, in an inverse manner as was done in (3), of weight vectors $W_v^x = (H^T V_{E^x}^{-1} H)^{-1} H^T V_{E^x}^{-1}$ and $W_v^y = (H^T V_{E^y}^{-1} H)^{-1} H^T V_{E^y}^{-1}$, respectively. The values of these weights are calculated in simulations at a subpupil level where the ‘‘true’’ tilt is known.

The total number of spatial frequencies involved in expression (5), N_f , mainly affects the computational cost of the algorithm, and it has also a certain influence over the tilt estimation performance. We have seen that a reasonably good performance is achieved with just six spatial frequencies². By limiting the $2D_FFT$'s computation in (2) to just the involved spatial frequencies, the computational cost of the WFPS algorithm is one order of magnitude smaller than the one required by the CC algorithm².

3. CAPACITIES ADDED TO THE OOMAO SIMULATOR

The Object Oriented Matlab toolbox for Adaptive Optics (OOMAO) is a freely available extension of the Matlab language, consisting of a library of Matlab classes oriented towards the numerical modelling of AO systems⁴. It has been used in the present work to simulate the WFPS algorithm performing in a SHWFS of an open loop configured AO system, and to compare its sensitivity with other known centroiding methods such as TCoG and CC.

OOMAO's object-oriented programming provides it with a modularity that facilitates the change of a particular aspect of the wavefront sensing subsystem, such as the centroiding method or the detector's gain and noise model in the SHWFS. Among the implemented classes, the *shackHartmann* class contains the necessary properties and methods to simulate the Shack-Hartmann wavefront sensor. The selection of the centroiding method is done through its properties, and the two implemented methods are the TCoG and the Quad Cell (QC). Since a SHWFS is composed basically of a lenslet array and a detector, two classes can be found embedded in the *shackHartmann* class: the *lensletArray* class, where the number of lenslets, number of detector pixels per lenslet, valid lenslets as a function of incident light, and spots size in pixels are defined; and the *detector* class, which implements the detector's gain and noise model, which consists of adding photonic noise to the light, adding a background light, applying a quantum efficiency and adding readout noise.

In the context of the present work, some features have been added to the *shackHartmann* class and its embedded *detector* class, necessary to achieve the desired simulation results. These have been the following:

1. The WFPS algorithm has been implemented in the *shackHartmann* class, at the *dataProcessing* method, where all the centroiding algorithms are to be found. Public properties *wfpsWeightsX* and *wfpsWeightsY* have been included to contain the Bayesian weights at the working spatial frequencies for the horizontal and vertical centroids calculation, respectively.
2. The CC centroiding algorithm has been implemented in the *shackHartmann* class. The correlation reference is the diffraction limited image, and is set with the *setCorrelationReference* method, which should be called after propagating a planar wavefront to the SHWFS. The correlation is executed in the Fourier domain, in the *dataProcessing* method. A thresholding can be applied to the correlation figure, through the *correlationThreshold* public property, and finally a centre of gravity is applied to the thresholded correlation figure. Resolution of the

correlation figure is kept the same as that of the live and reference images; interpolation of the correlation figure does not improve centroid estimation when a TCoG is applied to the same.

3. A gain and noise model of an Electron Multiplication Charge Coupled Device (EMCCD) detector has been implemented in the *detector* class. Figure 1 is a schematic representation of the main blocks in an EMCCD for a gain and noise statistical model derivation. The main difference with a Charge Coupled Device (CCD) detector is the inclusion of an Electron Multiplication (EM) register before the readout electronics, where the electrons are shifted using a higher clock voltage than in the detector array and readout register, in order to create more electrons through impact ionization.

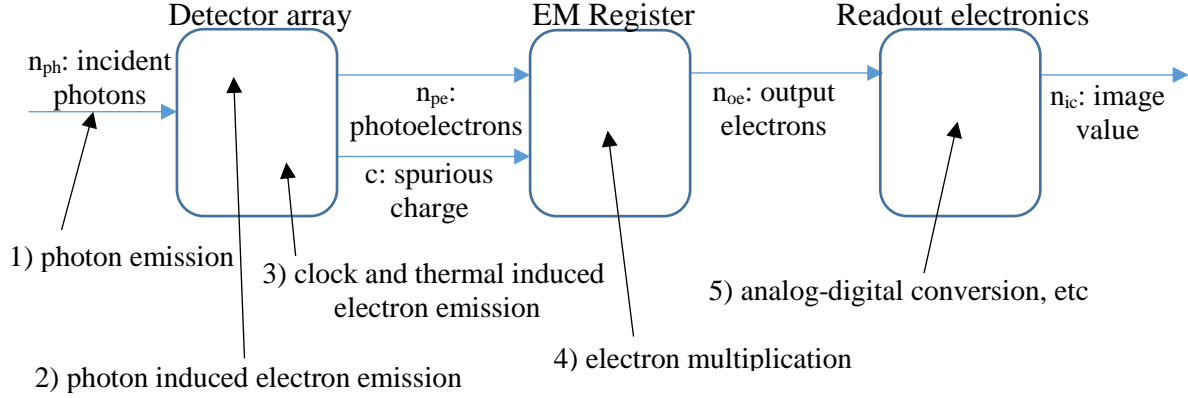


Figure 1. Block diagram of an EMCCD detector, from a gain and noise model point of view.

The employed stochastic model consists of the serial combination of three stochastic processes, corresponding to the three blocks in Figure 1: a Poisson process, a gamma process and a normal process⁵.

For a mean incident light intensity n_{ph} in photons, a quantum efficiency q and a mean spurious charge emission c measured in electrons, the latter consisting of both Clock Induced Charge (CIC) and thermally induced dark current during the exposure time, the probability of n_{ie} electrons entering the EM register can be expressed as a Poisson distribution with mean $qn_{ph} + c$, the sum of the mean generated photoelectrons $n_{pe} = qn_{ph}$ and the spurious charge:

$$p(n_{ie}; n_{ph}, q, c) = P(n_{ie}; qn_{ph} + c) \quad (6)$$

Expression (6) is the Poisson contribution to the end-to-end probability distribution of the proposed EMCCD model.

Impact ionization in the EM register is a stochastic process, and the probability to get n_{oe} output electrons from an EM register with mean gain value g and n_{ie} input electrons can be modelled by a gamma distribution:

$$p(n_{oe}; n_{ie}, g) = \gamma(n_{oe}; n_{ie}, g) = n_{oe}^{n_{ie}-1} \frac{e^{-n_{oe}/g}}{\Gamma(n_{ie})g^{n_{ie}}} \quad (7)$$

with n_{ie} the shape parameter and g the scale parameter in the gamma distribution. An exception is made to (7) when n_{ie} is zero, that is, no electrons enter the EM register, for which case the output n_{oe} is equalled to zero also. This means that the assumption is made that no electrons are created in the EM register for a null input, and that spurious charges are not created inside the EM register, which is only an approximation. Expression (7) is the gamma contribution to the overall statistical model for the EMCCD.

Finally, the readout electronics amplifies the signal and converts it into discrete image values n_{ic} , with a proportionality factor or sensitivity f , measured in electrons per ADU (Analog to Digital Unit) or image count. In this readout process, readout noise (RON) is introduced in the signal, which is modelled by a normal distribution with standard deviation r . Thus, the normal contribution to the EMCCD model can be expressed as:

$$p(fn_{ic}; n_{oe}, r) = N(fn_{ic}; n_{oe}, r) \quad (8)$$

with $N(fn_{ic}; n_{oe}, r)$ being the normal distribution of the process fn_{ic} , with n_{oe} mean value and standard deviation r . Ultimate quantization of n_{ic} into an integer value adds to the final total noise amount.

Public properties *emccdGain* and *CICNoise* have been added to the *detector* class to contain the EM gain and spurious charge per pixel per frame, respectively.

4. WORKFLOW AT THE OOMAO SIMULATION

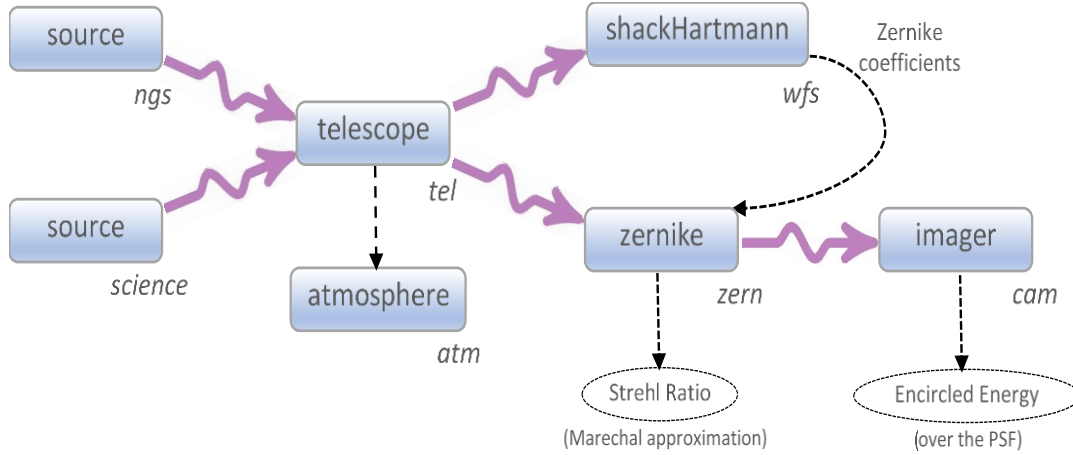


Figure 2. Core of the simulation workflow programmed in the OOMAO in the context of the present work

Figure 2 shows the objects involved and the optical paths connecting them in the context of the present work's OOMAO simulation. There are two optical paths that share a *telescope* instance with a 4.2 m. pupil diameter size and an 8.4% of central obscuration surface. The *telescope* instance embeds an *atmosphere* instance, which is initialized and configured following a model used in several examples included in the toolbox: a three-layer model with 0, 5 and 12 km. altitude and fractional r_0 's (Fried parameters) of 0.5, 0.3 and 0.2, respectively; wind speeds are 10, 5 and 20 m/s, and wind directions are 0, $\pi/2$ and π . Two overall Fried parameters are considered: 21 cm, the same size as the subpupil side, and 8.4 cm, which is 2.5 times smaller than the subpupil side. The system frequency has been set to 500 Hz.

Each optical path has its own source. The one labelled *ngs* represents the Natural Guide Star and its light ends up in the *shackHartmann* object. The second one, labelled *science*, represents the scientific object of interest and its light ends up in the *imager* object through a *zernike* object. Both light sources are set to the default wavelength of 550 nm, and therefore the system performance evaluation is made at the wavefront sensor (WFS) sensing wavelength. Also, both sources are located at the zenith, so no anisoplanatism error is being considered in the simulation.

The SHWFS observes the full dynamic range of the atmosphere, as in an open loop configuration. The *shackHartmann* object is configured to have a matrix of 20 x 20 square shaped lenslets, and only the subpupils with a minimum of 85% of light with respect to the most illuminated one are considered for the phase recovery computation. Sampling of the spots follows the Nyquist criterion. The number of detector pixels per lenslet has been set to 10 x 10 for the case of a 21 cm Fried parameter (r_0), making up a $\sim 2.7''$ FoV, and 14 x 14 for the case of an 8.4 cm r_0 , making up a $\sim 3.8''$ FoV. As regards the detector model, a quantum efficiency (QE) of 97% has been applied; star magnitudes under study are over 7.5, and an EMCCD gain value of 1000 has been applied; CIC noise has been set to 0.05 $e^-/\text{pixel}/\text{frame}$, and RON to 50 rms e^- . The sensitivity of the detector is the default 1 e^-/ADU . It is through the *shackHartmann* properties that the centroiding algorithm is selected: TCoG, CC or WFPS. As for the phase recovery at the whole pupil level, two cases are distinguished based of the amount of incident light level: when there are more than ~ 50 incident photons per subpupil for the TCoG algorithm or more than ~ 30 photons for the CC and WFPS algorithms, a zonal Linear Minimum Mean Square Error (LMMSE) method

estimates the phases at the subpupils' corners, and the Zernike modes are estimated by the pseudo-inversion of the matrix that relates modes with these phases; for dimmer situations, directly estimating the Zernike modes from the phase slopes, by pseudo-inversion of the matrix that relates modes with phase slopes, gives better results. The number of recovered Zernike modes that gives a best performance seems to depend mainly on the lenslet pitch and has been set to 130.

At the other optical path, an *imager* object receives a compensated wavefront. The corrector element is a *zernike* object that receives the corrective Zernike coefficient values from the *shackHartmann* instance. This correction is applied with the same spatial resolution in the pupil as the one defined in the *telescope* and *shackHartmann* objects, i.e., the number of lenslets multiplied by the number of detector pixels per lenslet. After this correction, the final Strehl Ratio (SR) can be easily calculated by the Marechal approximation, even before the computation of the Point Spread Function (PSF). An average residual phase is computed for this purpose, by integrating during a period of 4 seconds.

Finally, the *imager* object receives the wavefront with the residual phase, and integrates 200 frames with a temporal sampling period of 20 ms to compute the system PSF. Sampling is four times finer than the Nyquist criterion, i.e., the Full Width at Half Maximum (FWHM) of the PSF at diffraction limit is 8 pixels wide. The selected FoV is 50 times the FWHM at diffraction, 1.35" or 400 pixels, for the 21 cm r_0 case, and 125 times the FWHM at diffraction, 3.38" or 1000 pixels, for the 8.4 cm r_0 case, in order to span a ~95% of the PSF energy. By knowing the total light energy at the whole pupil, the Encircled Energy (EE) as a function of circle diameter in arcseconds can be computed over the PSF.

Magnitude 11, r_0 21 cm, G_{emccd} 1000, CIC 0.05 e^- , RON 50 rms e^- **Magnitude 11, r_0 8.4 cm, G_{emccd} 1000, CIC 0.05 e^- , RON 50 rms e^-**

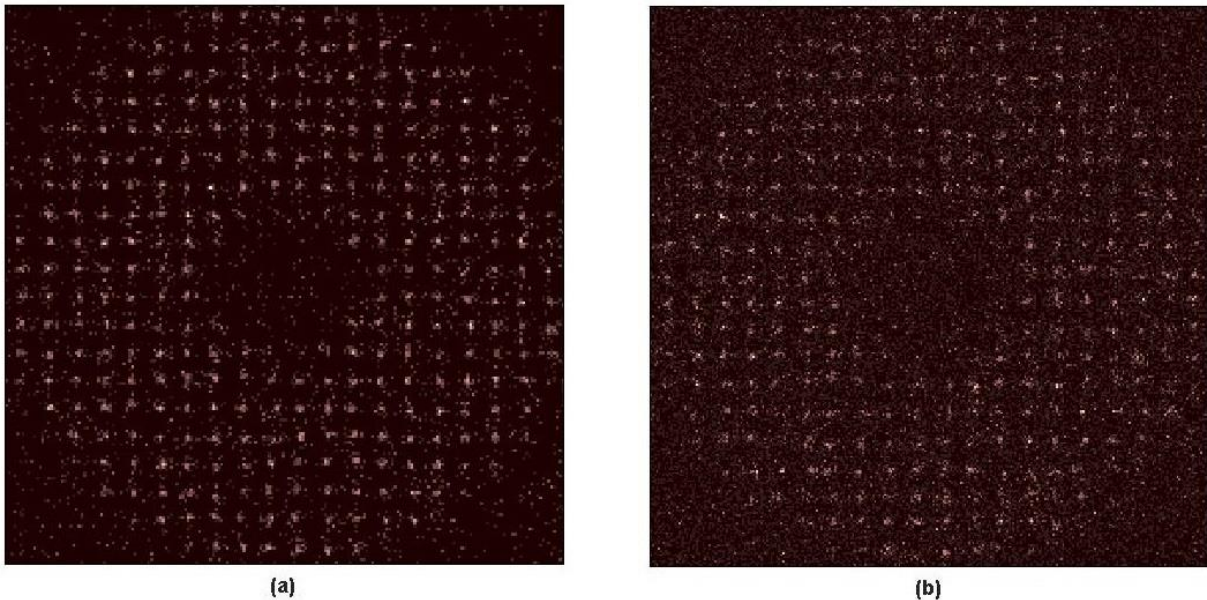


Figure 3. Samples of SHWFS images created with the OOMAO for a 20 x 20 subpupils configuration in a 4.2 m circular aperture with an 8.4% central obscuration and a magnitude 11 star. Nyquist sampling of the spots. (a) 21 cm r_0 , FoV of 10 x 10 pixels (~2.7" at 550 nm wavelength), EMCCD gain of 1000, CIC noise of 0.05 e^- /pixel/frame and RON of 50 rms e^- . (b) Same as in (a), for an 8.4 cm r_0 and 14 x 14 pixels FoV (~3.8" at 550 nm wavelength).

Figure 3 shows a couple of samples of the SHWFS detector's images created with the OOMAO simulator. The first panel, labelled (a), is for the 21 cm r_0 case and a star magnitude of 11, which for the default optical throughput of unity, means ~31.5 incident photons per subpupil at a system frequency of 500 Hz. FoV size is 10 x 10 pixels, which for a source wavelength of 550 nm and Nyquist sampling of the spot corresponds to a ~2.7" FoV. The EMCCD model has been applied, with gain and noise values as mentioned above and repeated in the figure's titles. RON noise is not actually visible in the figure. The spurious visible noise corresponds to CIC noise which, when amplified by the EM register, reaches habitual pixel peak values in the order of ~3000 – 5000 digital counts for the default detector sensitivity of 1 e^- /ADU, thus becoming noticeable against the spots' peak values of ~5000 – 10000 digital counts. In the second panel, labelled (b), the FoV has been increased to 14 x 14 pixels, corresponding to a ~3.8" FoV, in order to cope with the increase in turbulence strength of an 8.4 cm r_0 case. The spots are visibly more diffused and the image gives a global appearance of being noisier for the

same amount of incident light and added noise. The reader may note the importance of an appropriate detector gain and noise model. The EMCCD gain is a stochastic process that contributes, together with the atmospheric turbulence and Poisson noise, to deform the spots. Moreover, the spurious CIC noise cannot be modelled with an additive normal noise, such as is done for RON.

5. CENTROIDING METHODS COMPARED PERFORMANCE SIMULATION RESULTS

5.1 Strehl Ratio as a function of NGS magnitude

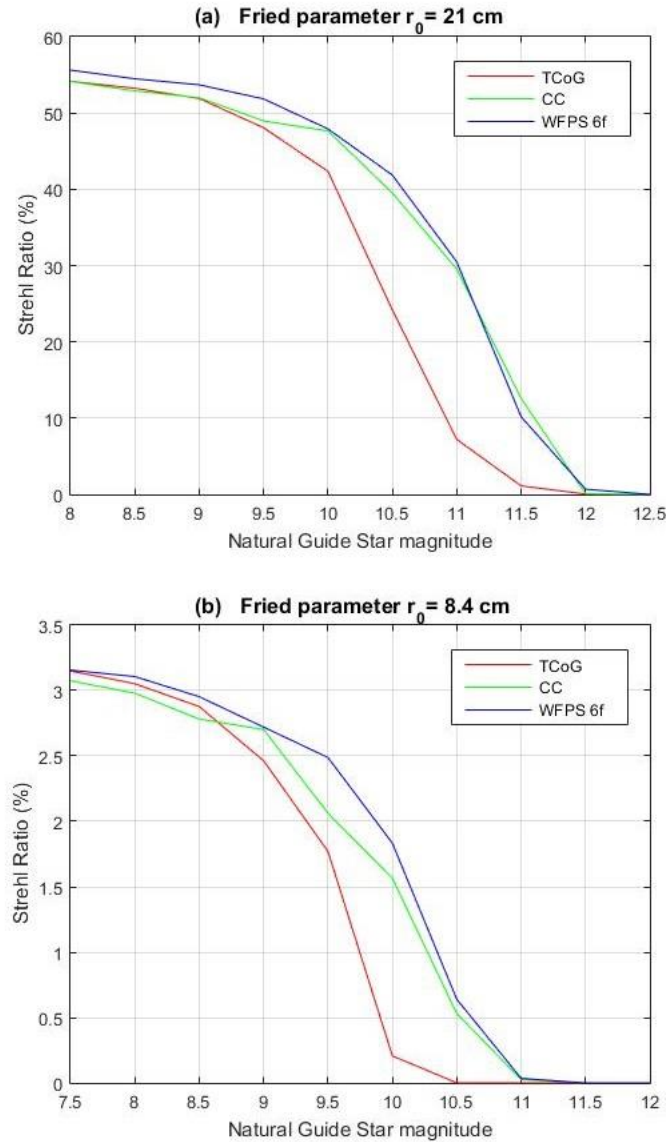


Figure 4. Strehl Ratio in percentage units, obtained by Marechal's approximation, as a function of star magnitude, for two atmospheric conditions: (a) 21 cm r_0 case and (b) 8.4 cm r_0 case; and three centroiding algorithms: TCoG (red traces), CC (green traces) and WFPS with 6 spatial frequencies (blue traces).

For the simulation configuration described in the previous section, Figure 4 shows results of achieved Strehl Ratio (SR) after turbulence compensation as a function of the NGS magnitude, for three centroiding algorithms under study: TCoG (red traces), CC (green traces) and WFPS involving six spatial frequencies (blue traces), all tuned to estimate Z-Tilt at the

subpupil*; and two atmospheric conditions: panel (a) shows the results for a 21 cm r_0 case, and results for a 8.4 cm r_0 case are shown in panel (b). From these results we can see that CC and WFPS algorithms show a similar sensitivity behaviour, outperforming the TCoG algorithm by increasing the limiting NGS magnitude for a particular achieved SR. The range of incident light where this improvement occurs depends on the atmospheric condition and goes from a star magnitude of 8.5 – 9, which corresponds to 300 – 200 incident photons, till the SR falls to near zero value at magnitude 11 – 12, corresponding to 30 – 12 photons. In the central zone of this range, the difference in star magnitude between TCoG and WFPS algorithms for a particular SR performance is ~ 0.6 to ~ 0.7 .

5.2 Encircled Energy as a function of NGS magnitude

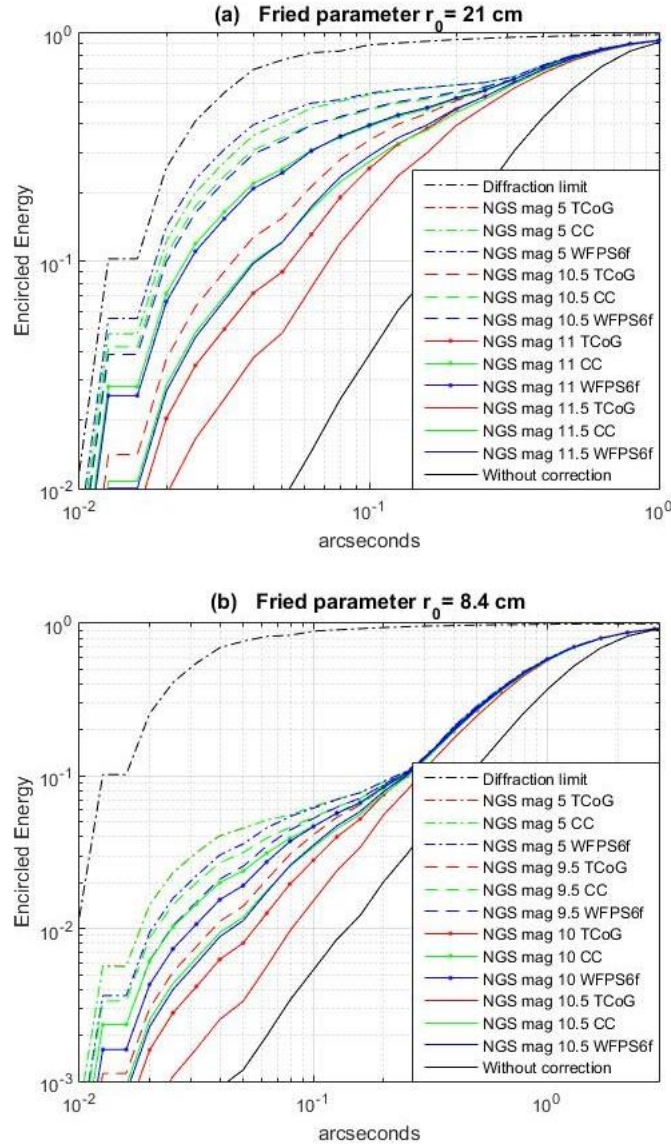


Figure 5. Encircled Energy graphs as a function of star magnitude for two atmospheric conditions: (a) 21 cm r_0 and (b) 8.4 cm r_0 ; and three centroiding algorithms: TCoG (red traces), CC (green traces) and WFPS with 6 spatial frequencies (blue traces), all tuned to estimate G-Tilt. Diffraction limited and no correction cases are shown in black traces.

* It has been seen that Z-Tilt estimation at the subpupil level leads to a higher SR at a pupil level, whereas G-Tilt estimation leads to a higher EE at a pupil level²

When centroiding algorithms are tuned to estimate G-Tilt at the subpupil level, the figure of merit we choose to assess the algorithm's performance is the Encircled Energy (EE) as a function of spanned FoV, calculated over the PSF that the *imager* object gives. Figure 5 shows these EE graphs in a double logarithmic scale, with panel (a) corresponding to the 21 cm r_0 case and panel (b) corresponding to the 8.4 cm r_0 case. TCoG results for various NGS magnitudes are shown in red traces with different line styles; the same magnitudes and line styles for the CC algorithm are shown in green traces; and blue traces are used for the WFPS algorithm. For a comparison purpose, the diffraction limited case and the turbulence uncompensated case are shown in black traces as best and worst limits, respectively.

Results are in good agreement with the SR's shown in Figure 4. For a bright NGS of magnitude 5, the performance is similar for the three algorithms, with the red trace of the TCoG being right underneath the green trace of the CC, and thus being not visible. For higher NGS magnitudes, all the EE graphs approach the uncorrected performance, with the CC and WFPS algorithms behaving similarly to each other, and the TCoG requiring a brighter NGS of ~ 0.75 lower magnitude to achieve the same performance as the other two algorithms. For higher than 0.15" spanned FoV's, the WFPS gives the highest EE values of the three algorithms.

6. CONCLUSIONS AND FUTURE WORK

The Weighted Fourier Phase Slope (WFPS) algorithm has been presented as a new centroiding method for SHWFS's that operates in the Fourier domain, obtaining the image displacement from the Fourier phase slopes through a Bayesian estimation.

This algorithm has been introduced in the OOMAO simulator, and an open loop correction simulation has been conducted that takes into account only the measurement error at the subpupil level and the sensor's fitting error at the whole pupil's level. The performance of three algorithms, TCoG, CC and WFPS have been compared. In high light level scenarios, that is, when fitting error dominates, all the algorithms perform similarly. When measurement noise at subpupil level dominates, that is, at low light level scenarios, CC and WFPS allow to use dimmer NGS's, of about ~ 0.6 to ~ 0.7 higher magnitudes, than the required by the TCoG algorithm, for a certain performance as measured by a SR or an EE. The WFPS algorithm has been tested spanning only six spatial frequencies, and this means a significant reduction in computational cost with respect to the CC.

This study has been reported for a 4.2 m circular aperture with 8.4% central obscuration, which are the William Herschel Telescope's dimensions. A 20 x 20 matrix of square shaped subapertures has been considered for wavefront measurement at the SHWFS. And two turbulence strength conditions have been simulated: a 21 cm r_0 , equal to the subaperture side size, and an 8.4 cm r_0 , 2.5 smaller than the subaperture side size.

Future work may be directed towards completing the simulation by introducing the effect of the computational latency of the centroiding algorithms over the final atmospheric phase compensation. Also, assessing the performance degradation due to the variation of observational conditions, such as Fried parameter or guide star incident light, with respect to the nominal values used for the tuning of the algorithms, would be of interest in order to specify the required refreshment period in an on-sky observation of the algorithms' parameters (Bayesian weights for the WFPS algorithm).

ACKNOWLEDGEMENTS

This work has been partially funded by the National R&D Program of the Ministry of Economy and Competitiveness (Project DPI2015-66458-C2-2-R), CIBICAN and the European Regional Development Fund (ERDF). Haresh Chulani would like to also thank the Instituto de Astrofísica de Canarias' Technology Division for financing his AO4ELT5 Meeting related expenses.

REFERENCES

- [1] Chulani H. M. and Rodríguez-Ramos J. M., "Weighted Fourier Phase Slope as a centroiding method in a Shack-Hartmann wavefront sensor: A Z-tilt estimation method in the Fourier domain, optimizable to the system's geometry", IEEE 12th Workshop on Information Optics (WIO'2013).

- [2] Chulani H. M., “Weighted Fourier Phase Slope as a Centroiding Method in a Shack-Hartmann Wavefront Sensor for Adaptive Optics in Astronomy”, PhD Dissertation, University of La Laguna, Spain. June, 2017.
- [3] Oppenheim A. V. and Schafer R. W., [Discrete Time Signal Processing], Prentice Hall International, Inc (1989).
- [4] Conan R. and Correia C., “Object-oriented Matlab adaptive optics toolbox”, Adaptive Optics Systems IV, Proc. SPIE 9148.
- [5] Hirsch M. et al, “A Stochastic Model for Electron Multiplication Charge-Coupled Devices – From Theory to Practice”, PLoS ONE, Vol 8, Issue 1: e53671